arXiv:cond-mat/0403544v2 [cond-mat.mtrl-sci] 23 Mar 2004

Cold neutron scattering study on the diffuse and phonon excitations in the relaxor $Pb(Mg_{1/3}Nb_{2/3})O_3$

H. Hiraka[1,2], S. -H. Lee[3], P. M. Gehring[3], Guangyong Xu[1], and G. Shirane[1]
[1]*Department of Physics, Brookhaven National Laboratory, Upton, New York 11973*
[2]*Institute for Materials Research, Tohoku University, Sendai 980-8577, Japan*
[3]*NIST Center for Neutron Research, National Institute of Standards and Technology, Gaithersburg, Maryland 20899*
(Dated: March 22, 2022)

Cold neutron scattering experiments have been performed to explore the energy, temperature, and wave-vector dependence of the diffuse scattering and the transverse acoustic (TA) phonons in the relaxor $Pb(Mg_{1/3}Nb_{2/3})O_3$. We have observed a weak, but definitive, diffuse scattering cross section above the Burns temperature $T_d \sim 600$ K. This cross section, which is most likely caused by chemical short-range order, persists down to 100 K, and coexists with the much stronger diffuse scattering that is attributed to the polar nanoregions. A systematic study of the TA phonon around $(1,1,0)$ has also been carried out. The phonon is well defined for small wave vectors $\mathbf{q}$, but broadens markedly around $\mathbf{q} = (0.1, -0.1, 0)$.

PACS numbers:

I. INTRODUCTION

The lead-oxide perovskite $Pb(Mg_{1/3}Nb_{2/3})O_3$, or PMN, is one of the most interesting and well-studied relaxor compounds to date, primarily because of its exceptional piezoelectric properties and enormous potential in industrial applications[1,2]. Neutron scattering has played a particularly important role in the study of the unusual lattice dynamics and diffuse scattering observed in single crystals of PMN[3,4,5,6,7,8,9]. Because of the Q^2-dependence of the phonon and diffuse scattering cross sections, most studies to date have made use of thermal neutrons ($\lambda \sim 2$ Å) in order to access Brillouin zones corresponding to large momentum transfer $\mathbf{Q}$. However, Xu *et al.* have performed recent experiments on PMN using cold neutron ($\lambda \geq 4$ Å) time-of-flight (TOF) techniques that have succeeded in observing the diffuse scattering in the low-$\mathbf{Q}$ $(1,0,0)$ Brillouin zone[10]. Other cold neutron studies have also reported diffuse and low-energy TA phonon measurements made at low-$\mathbf{Q}$[11,12,13].

In this paper we report cold neutron scattering experiments on PMN using triple-axis spectroscopic techniques. Our goal was to explore the static and dynamic relaxor properties of PMN through measurements of the diffuse scattering and the transverse-acoustic (TA) phonons at small reduced wave-vector $\mathbf{q}$ in the $(1,0,0)$ and $(1,1,0)$ zones. The diffuse scattering in PMN is believed to be directly associated with the formation of polar nanoregions (PNR) at the Burns temperature ($T_d \sim 600$ K[14]), and it increases rapidly with cooling[3,9]. This diffuse scattering keeps increasing through the ferroelectric transition temperature ($T_C \simeq 210$ K[5,15,16]). Careful examination confirms the presence of a very weak, but definitive, diffuse scattering cross section above T_d. The high-temperature contours of this scattering are quite different in shape from those observed at low temperatures[8,9,10,17,18,19]. These contours persist to lower temperatures, remaining unchanged even after the much stronger low-temperature diffuse scattering sets in. The high-temperature contours are therefore very likely related to the atomic shifts produced by the underlying chemical short-range order intrinsic to PMN.

The use of cold-neutron wavelengths limits our measurements to the $(1,0,0)$ and $(1,1,0)$ zones. Moreover, the TA phonon measurements are only possible in the $(1,1,0)$ zone because the dynamical structure factor of the TA phonon is nearly zero at $(1,0,0)$ (see Table I). A well-defined low-energy TA phonon mode is observed at the smallest $\mathbf{q}$, or $\zeta = 0.035$, near $(1,1,0)$ over a wide range of temperatures, where $\mathbf{q} = (\zeta, -\zeta, 0)$. During the course of our experiments, Stock *et al.* reported a dramatic line broadening of TA phonon for $T_C < T < T_d$ in the same $(1,1,0)$ zone at $\zeta = 0.1$ or higher[20]. Therefore, we have extended our cold-neutron measurements up to $\zeta = 0.1$ for temperatures around T_d as well as below T_C. Our results overlap and agree with their thermal neutron data.

II. EXPERIMENTAL DETAILS

Our experiments were carried out on the cold neutron triple-axis spectrometer SPINS located at the NIST Center for Neutron Research. The PMN sample, grown at Si-

TABLE I: Calculated structure factors for PMN. For $|F_{soft}|^2$, the parameter S_2/S_1 is fixed to be 1.5 according to Ref. 9. See the text for $|F_{diff}|^2$.

—	Bragg	TA phonon	Soft phonon	Diffuse
(hkl)	$\lvert F_B\rvert^2$	$Q^2\lvert F_B\rvert^2$	$Q^2\lvert F_{soft}\rvert^2$	$Q^2\lvert F_{diff}\rvert^2$
(100)	1	0.2	11	11
(110)	9	5	9	32
(111)	37	28	37	2
(200)	100	100	91	0.1
(300)	1	2	100	100

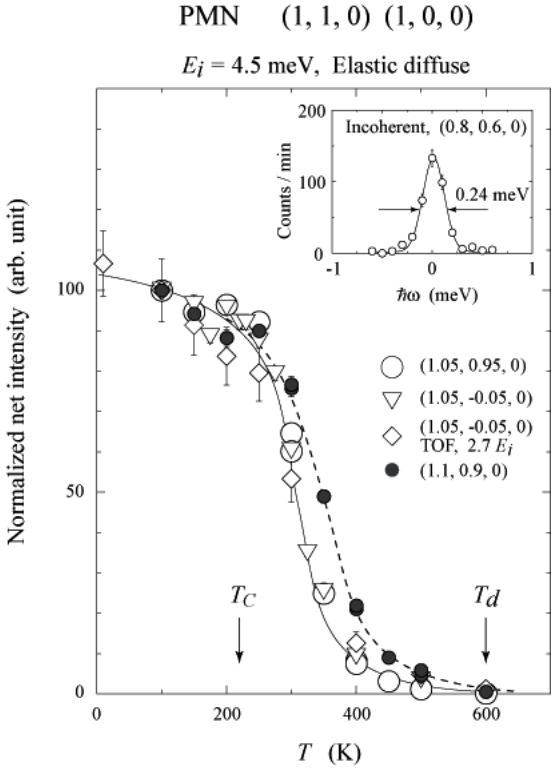


FIG. 1: Temperature dependence of the elastic diffuse scattering intensity measured at $\zeta = 0.05$ and 0.1. Data are normalized at 100 K. The solid and broken lines are guides to the eyes. Open diamonds show the results from TOF measurements[10].

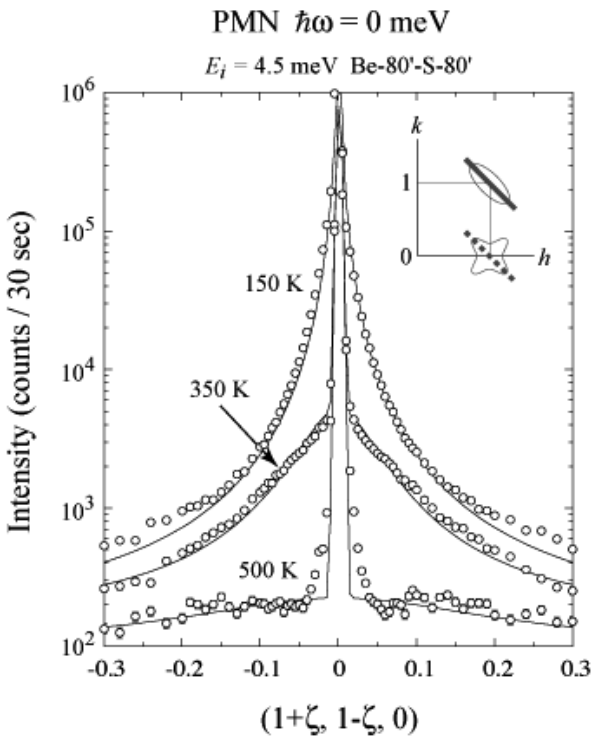


FIG. 2: Thermal evolution of the elastic diffuse scattering around $(1, 1, 0)$ along the intensity "ridge" direction (thick line, inset).

mon Fraser University in Canada, has a mass of 4.8 grams and is the same high-quality single crystal that was studied in previous reports[5,6]. The sample has a room-temperature lattice parameter of 4.04 Å, so that 1 rlu (reciprocal lattice unit) = 1.56 Å^{-1}. The crystal [001] axis was mounted vertically so that data were collected in the $(h, k, 0)$ scattering plane. The initial (final) neutron energy E_i (E_f) was fixed at 4.5 meV ($\lambda = 4.26$ Å and $k = 1.47$ Å^{-1}) during elastic (inelastic) neutron measurements, and a Be filter was placed before (after) the sample to remove higher order neutrons. The $(0, 0, 2)$ reflection of highly-oriented pyrolytic graphite crystals was used to monochromate and analyze the incident and scattered neutron energies, respectively. The beam collimations employed were guide-80'-80'-open. The measured instrumental energy resolution for this configuration is $2\Gamma_{res} = 0.24$ meV as shown in the inset of Fig. 1, and the background level is about 4 counts per minute.

III. ELASTIC DIFFUSE SCATTERING

Motivated by recent TOF measurements on PMN[10], we have performed a systematic investigation of the diffuse scattering around both of the $(1, 0, 0)$ and $(1, 1, 0)$ Bragg peaks. The temperature dependence of the diffuse scattering intensity is plotted in Fig. 1 at several different $\mathbf{Q} = \mathbf{G} + \mathbf{q}$ positions, where $\mathbf{G}$ represents either the $(1, 1, 0)$ or $(1, 0, 0)$ reciprocal lattice vector and $\mathbf{q} = (\zeta, -\zeta, 0)$. All intensities have been normalized to 100 at 100 K. The open-symbol data were measured at the same $\zeta = 0.05$. We first note that the thermal evolution of the diffuse scattering intensity is very similar around different Bragg peaks. Another interesting point is that while the diffuse scattering intensity is visible just below T_d, it grows rapidly below $\sim$ 400 K. This result is in good agreement with previous high-resolution TOF measurements, which are shown by the open diamonds in Fig. 1[10]. In the TOF study the instrumental energy resolution ($E_i = 2.7$ meV and $2\Gamma_{res} = 0.085$ meV) was about three times better than that of the SPINS experiment. The consistency between these independent measurements is significant because it shows that the data do not change with improving energy resolution. Thus our data render an accurate portrayal of the intrinsic temperature dependence of the elastic diffuse scattering. At larger $\mathbf{q}$, such as $\zeta = 0.1$, which is shown by the solid circles in Fig. 1, the diffuse scattering intensity takes off at a slightly higher temperature, so the whole curve (broken line) is shifted toward higher temperatures. However the overall behavior is still the same, i.e. the diffuse scattering intensity is always first detected at or just below T_d,

and increases monotonically with cooling.

Typical **q**-profiles of the elastic diffuse intensity measured around the $(1,1,0)$ peak are shown in a semi-log plot in Fig. 2. The intensity profiles are well described by a Gaussian function (Bragg peak) plus a Lorentzian function (diffuse scattering) and a flat background. The fits are shown as the solid lines in Fig. 2. With increasing temperature, the intensity of the diffuse scattering decreases, and the width of the Lorentzian increases, indicating a decrease in the correlation length. This temperature variation agrees with that measured in the $(1,0,0)$ zone along the same $[1\bar{1}0]$ direction[10] (broken line, in the inset of Fig. 2). Note that the diffuse intensity becomes very weak even at 500 K, which is still 100 K below T_d.

Intensity contours of the diffuse scattering measured at 300 K and 650 K are shown in Fig. 3. At 300 K, which is above T_C, but below T_d, the scattering is strong in both zones, and in agreement with previous studies [8,9]. The scattering intensity forms a "butterfly" pattern around the (1,0,0) Bragg peak, with ridges extending along the $[1\ \pm 1\ 0]$ directions. The scattering at $(1,1,0)$ is ellipsoidal in shape, and extends along the $[1\ \bar{1}\ 0]$ direction. These results are consistent with previous x-ray[17,18,19] and neutron[8,9,10] measurements. On the other hand, a weak pattern of diffuse scattering is still visible around both of these Bragg peaks at 650 K, just above T_d [Figs. 3 (c) and (d)]. This high-temperature scattering exhibits a geometry that is quite different from that observed at 300 K. The intensity of the high-temperature diffuse scattering at $(0.9,0.9,0)$ in Fig. 3 (c), for example, is less than 0.1 % of that of the low-temperature diffuse peak at $(1,1,0)$.

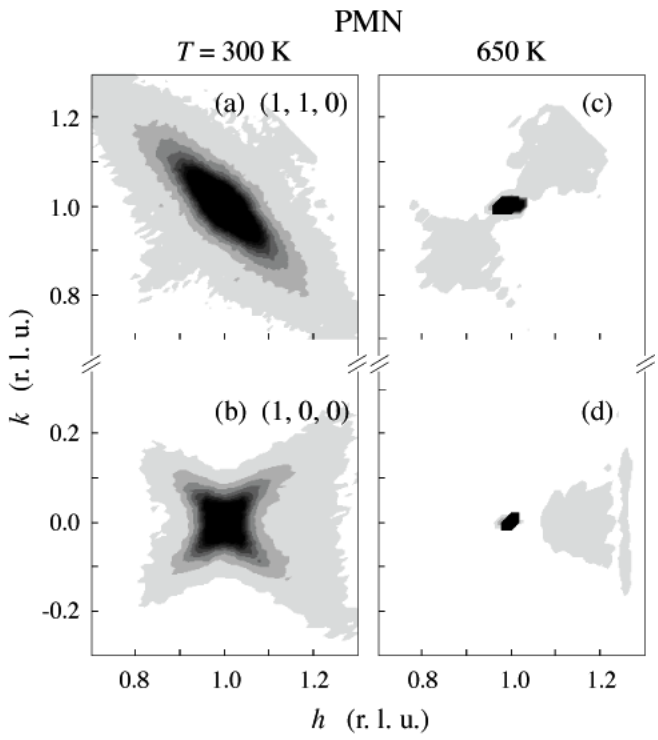


FIG. 3: Intensity contours of the elastic diffuse scattering well below T_d (left column) and just above T_d (right column), around the $(1,0,0)$ and $(1,1,0)$ Bragg peaks.

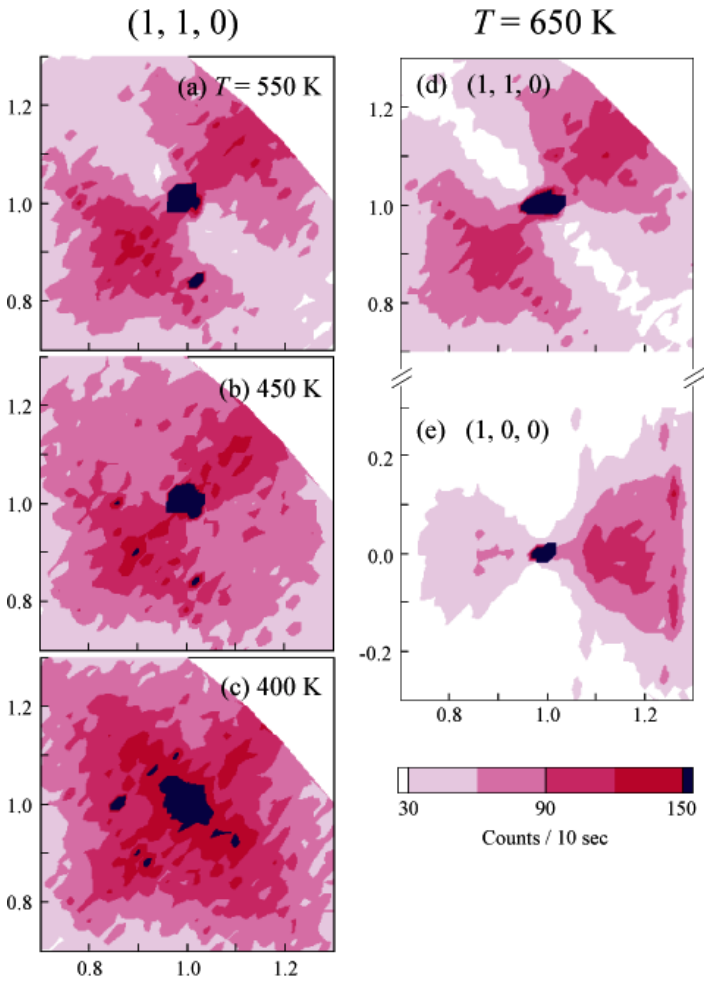


FIG. 4: Temperature variation of diffuse scattering contours near $(1,1,0)$. The background level is ~ 20 counts per 10 sec. Tuned high-temperature contours measured at 650 K in (d) $(1,1,0)$ and (e) $(1,0,0)$ zones.

The presence of a diffuse cross section above T_d is very surprising. Therefore, we did an extra background check using a single crystal of $SrTiO_3$ (~ 2 cc) and the identical configuration as used with PMN. No meaningful signal was observed near $(1,0,0)$ and $(1,1,0)$ within the experimental accuracy.

In Fig. 4, the intensity scale was tuned to better illustrated the contrast of the high-temperature diffuse contour (HTC). The intensity level of the HTC is much weaker than that of the low-temperature diffuse peak associated with the PNR formation as listed in Table II. However, because of the clean window and the efficiency of the spectrometer, the signal to noise ratio reaches about 4 even in the weak HTC. The HTC have distinctly

TABLE II: Observed peak intensity (counts/min).

—	(1,0,0)	(1,1,0)
Bragg	1.2×10^6	2.0×10^6
100-K Diffuse	9×10^5	6×10^5
650-K HTC	500	500
Incoherent	130	—
Background	4	—

different shapes than the low temperature diffuse intensities in both $(1,1,0)$ and $(1,0,0)$ zones. They seem to peak at incommensurate positions around (1.1,0,0) and (0.9,0,0) in the $(1,0,0)$ zone, and (1.1,1.1,0) and (0.9,0.9,0) in the $(1,1,0)$ zone, while the low temperature diffuse scattering intensities always reach the maximum at the zone center $\mathbf{q} = 0$. The intense spots at the center of the contour plots are scattering intensities from the Bragg peak. On cooling, around 450 K, the HTC can be clearly seen, superimposed with the increasingly strong low temperature diffuse cross section [see Figs. 4 (a) - (c)]. The weak HTC are further seen down to even lower temperatures in Figs. 3 (a) and (b), and virtually unchanged below 650 K. Details on this high temperature diffuse cross section will be further discussed in the discussion section.

IV. PHONON AND BROAD DIFFUSE SCATTERING

To date the transverse acoustic (TA) phonons in PMN have mainly been studied using thermal neutrons. All measurements are in good agreement in the $(2,0,0)$ and $(2,2,0)$ zones[3,4,5,6] where diffuse scattering is very weak (see Table I). Naberezhnov *et al.*[3] discovered that the TA-phonon starts to broaden at T_d. Later on, Wakimoto *et al.*[5] found this slight broadening disappears at T_C. However, pronounced TA-phonon anomalies were observed in $(3,0,0)$ and $(1,2,2)$ zones[3,6,7], where the diffuse cross section is large (see Table I). These anomalies were interpreted as the results of different types of phonon interactions. Our current measurements are limited in small $\mathbf{Q}$ zones as a result of the scattering geometry for cold neutrons, and are centered around $(1,1,0)$. $(1,1,0)$ is a good zone to study both TA phonon and diffuse scattering, because interaction from the soft transverse-optic (TO) phonon must be very weak due its small cross section.

The fine energy resolution intrinsic to cold neutron experiments ($E_f \sim 4$ meV and $2\Gamma_{res} \sim 0.2$ meV for typical triple-axis measurements) has the great advantage of enabling the measurement of low-energy excitations at small $\mathbf{q}$. To clarify the relationship between the diffuse scattering and the TA phonon in PMN, the dynamic scattering function $S(\mathbf{q},\omega)$ was studied along the strong diffuse intensity ridge $\mathbf{q} = (\zeta, -\zeta, 0)$ for $0.035 \leq \zeta \leq 0.1$. The TA-phonon structure factor at $(1,1,0)$ is much larger than that at $(1,0,0)$, as demonstrated in Table I. The diffuse scattering structure factor $Q^2|F_{diff}|^2$ listed there is calculated from the atomic shifts derived from neutron diffuse scattering measurements by Vakhrushev *et al.*[8]

Energy spectra measured at $\zeta = 0.035$ for several different temperatures are shown in Fig. 5. A well-defined TA phonon mode is observed at the smallest $\mathbf{q}$ over a wide range of temperatures in spite of the relatively small value of $\mathbf{Q}$ and the small resolution volume. At 400 K the energy spectrum shows an interesting and definite overlap of the TA phonon with the central diffuse scattering intensity. This overlap could be the result of a softening of the TA phonon energy and the prominent tail of the elastic central peak. This suggests that extra spectral weight exists in the central peak in addition to the resolution-limited elastic diffuse intensity. A small

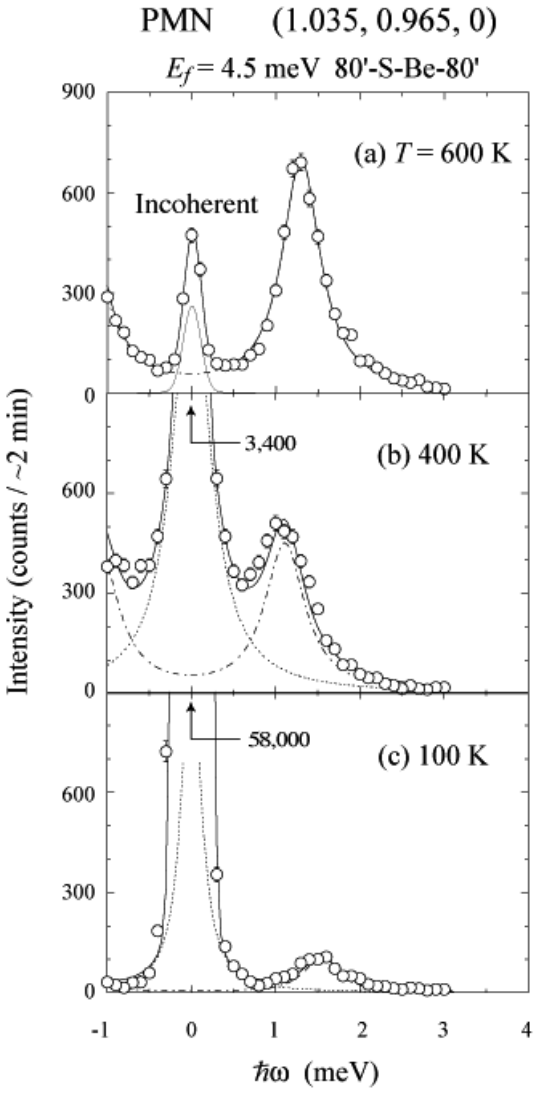


FIG. 5: Temperature variation of constant-$\mathbf{Q}$ scans measured at small $\mathbf{q}$ near (1,1,0). Fits are described in the text.

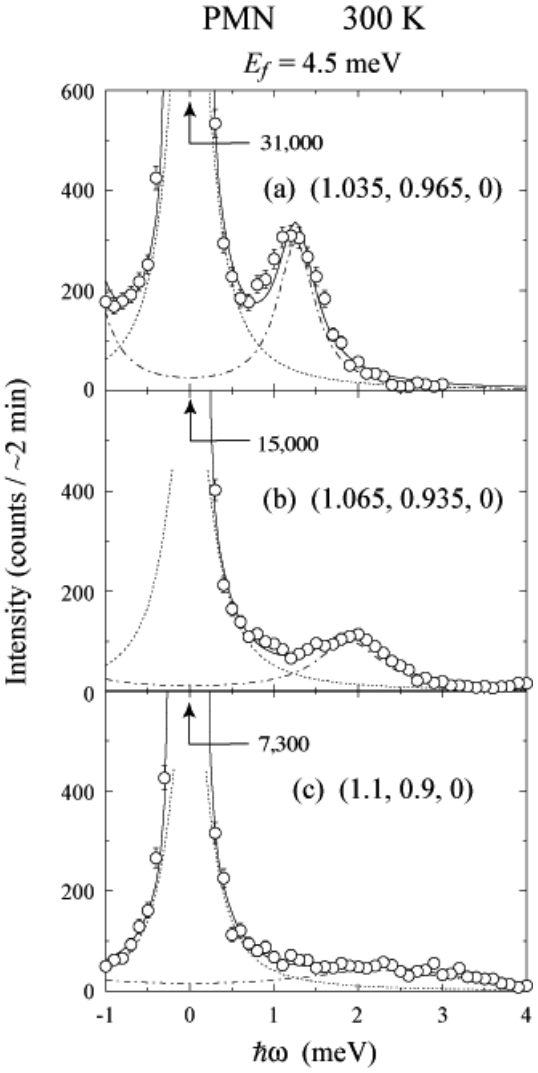


FIG. 6: **q** variation of constant-**Q** scans measured at 300 K near (1,1,0).

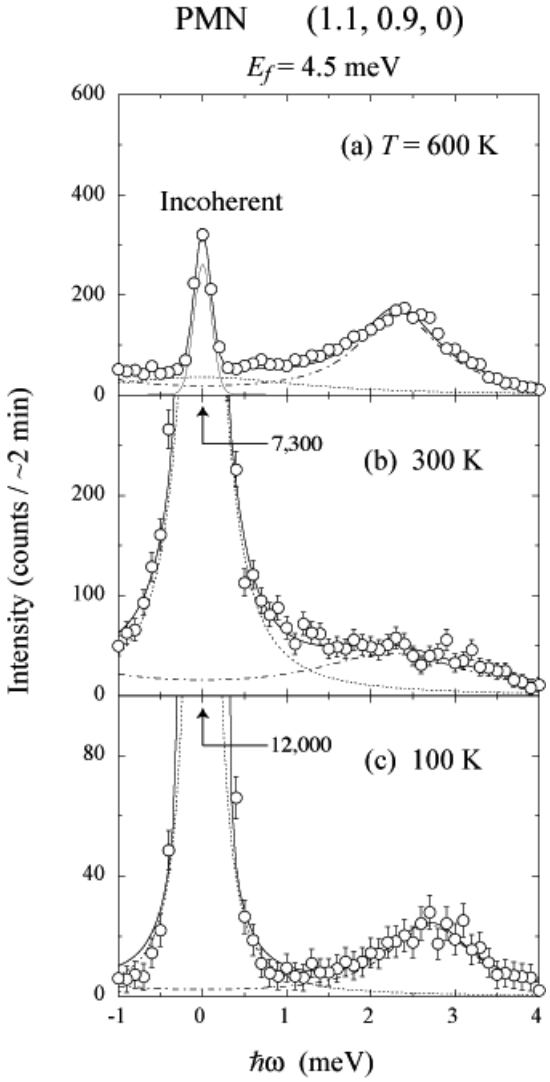


FIG. 7: Constant-**Q** scans at $\zeta = 0.1$ for three temperatures. The incoherent scattering is shown by a thin line only in (a).

portion of the diffuse tail still remains at 100 K, but completely disappears at 600 K. From these data we conclude that no elastic diffuse scattering is present at 600 K at this **q**.

Energy spectra measured at 300 K and for **q** up to $\zeta = 0.1$ are shown in Fig. 6. The overlap of the TA phonon with the broad central peak is still evident in this region. It is interesting to note that the TA phonon broadens markedly with increasing **q** at 300 K, as is quite apparent at $\zeta = 0.1$. In order to overlap with the thermal neutron measurements of Stock *et al.*[20], we have carried out further measurements at $\zeta = 0.1$ for 600 K ($\sim T_d$) as well as 100 K ($\ll T_C$). Figure 7 traces the evolution of the TA phonon at $(1.1, 0.9, 0)$. The broadening reaches a climax at the intermediate temperature 300 K. At $T =$ 100 K, which is well below T_C, the TA phonon at $\zeta = 0.1$ almost recovers its original line shape.

In the course of the current data analyses for energy spectra typically shown in Figs. 5 - 7, we used the following scattering function to fit :

$$S(\mathbf{q},\omega) = S_{rlD} + S_{brD} + S_{TA}. \tag{1}$$

Here, S_{rlD} represents the resolution-limited elastic diffuse peak and it is expressed as a Gaussian function with the full width of $2\Gamma_{res}$ as previously done[3,7,12,13]. S_{brD} is the broad diffuse scattering prominent for intermediate temperatures $T_C < T < T_d$. S_{TA} describes the TA phonon scattering. We model S_{brD} and S_{TA} in the following way:

$$S_{brD} \sim \frac{\Gamma_{diff}}{\omega^2 + \Gamma_{diff}^2}, \tag{2}$$

$$S_{TA} \sim \frac{\Gamma_{TA}}{(\omega - \omega_{TA})^2 + \Gamma_{TA}^2}. \tag{3}$$

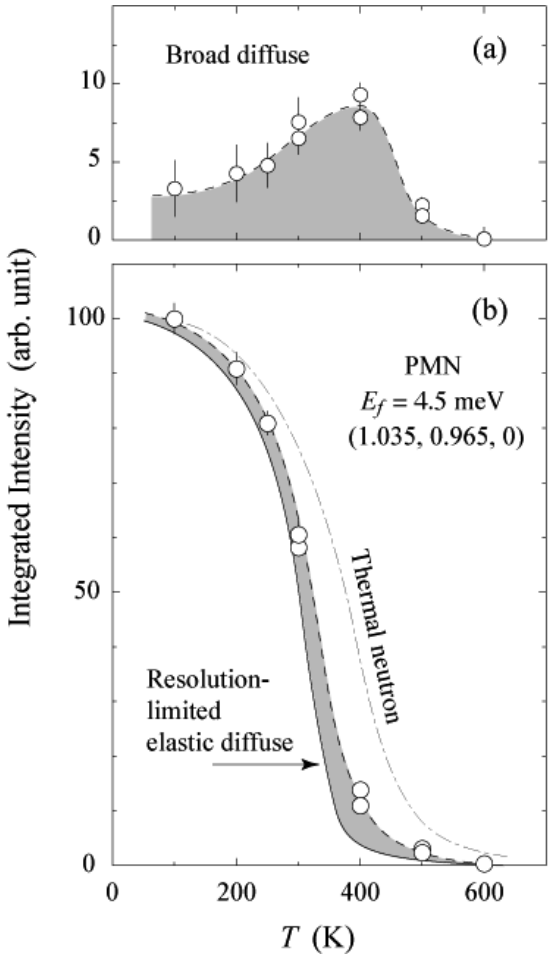


FIG. 8: The energy-integrated intensity of the diffuse scattering as a function of temperature. The shaded region represents the contribution from the broad central component. The resolution-limited elastic component is shown by the solid line. All curves are guides to the eye.

In this model we regard the broad diffuse scattering as a part of intrinsic cross section for PNR.

These functional forms in Eqs. (1) - (3) fit the data quite well as shown by the solid lines in Figs. 5 - 7, where the phonon and the broad central diffuse component are depicted by the chained and dotted lines, respectively. Fitting parameters at $\zeta = 0.035$ and 0.1 for three temperatures are listed in Table III. $|F_{TA}|$ is derived from the scale factor for Eq. 2 after removing the prefactor of phonon intensity (T/ω_{TA}^2). The peculiar broadening of the TA phonon is supported numerically in Γ_{TA} at $\zeta = 0.1$ for $T_C < T < T_d$. In contrast, the TA-phonon mode at $\zeta = 0.035$ is well behaved for a wide range of temperatures with the nearly temperature-independent linewidth and the dynamical structure factor.

The temperature dependence of the energy-integrated intensity of the diffuse scattering at $\zeta = 0.035$ (I_{diff} in Table III) is shown in Fig. 8. The broad central component measured at the smallest $\mathbf{q}$ peaks around 400 K,

TABLE III: Representative fitting parameters without resolution corrections. I_{diff} and $|F_{TA}|$ are related to the scale factors in Eqs. (2) and (3), respectively.

ζ (rlu)	T (K)	ω_{TA} (meV)	$\lvert F_{TA}\rvert$ —	$2\Gamma_{TA}$ (meV)	$2\Gamma_{diff}$ (meV)	I_{diff} —
0.035	100	1.6	100	0.6	0.3	3
0.035	300	1.2	80	0.6	0.4	8
0.035	600	1.3	90	0.5	—	0
0.1	100	2.7	150	1.6	0.3	7
0.1	300	2.3	110	2.4	0.5	19
0.1	600	2.3	110	1.2	2.8	6

reaching about 10 % of the low-temperature resolution-limited elastic value (shaded region in Fig. 8). Below 400 K, which is far below T_d, the sharp elastic component grows quickly and becomes dominant [see Fig. 8 (b)]. As reported in previous papers[3,9], the diffuse scattering intensity, corresponding to the formation of PNR, begins to develop around T_d when observed with thermal neutrons as schematically shown in Fig. 8 (b). The difference between the thermal and cold neutron results can then be naturally attributed to differences in the experimental resolution functions.

V. DISCUSSION

The most important new result of the current experiment is the observation of the HTC in Figs. 4 (d) and (e). The scattering pattern is longitudinal to $\mathbf{Q}$. Also the intensity at larger $\mathbf{Q}$ is stronger than that at smaller $\mathbf{Q}$ [Fig. 4 (e)], consistent with diffuse scattering resulting from atomic shifts, where $I \propto |\mathbf{Q} \cdot \epsilon|^2$. Theoretical studies[21,22] have suggested that short-range chemical order between Mg^{2+} and Nb^{5+} ions at the perovskite B-sites should generate local electric field that leads to shifts of the A-site Pb^{2+} ions. This short-range chemical order is believed to be temperature insensitive up to $T \sim 1000$ K. We speculate that this broad incommensurate cross section in the HTC reflects atomic shifts that modulate in the longitudinal direction, caused by the short-range chemical order. These atomic shifts are also short-range correlated, resulting in the diffuse type scattering pattern around the incommensurate positions. Finally, the shape of the HTC looks somewhat conjugate with that of the low-temperature strong diffuse cross section. This may be more than merely a coincidence. It is likely that the diffuse contours from the PNR grow out of the HTC with cooling, but this is just a conjecture at present.

In the diffuse-phonon-profile analysis of the $(1, 1, 0)$-zone data, the additional broad diffuse cross section of S_{brD} was interpreted as the part of intrinsic dynamics of PNR. It is the same approach employed by Gvasaliya *et al.*[12,13] This broad Lorentzian cross section may contain intensity transferred from the TA phonon by coupling

to the resolution-limited elastic peak[23]. So far we could not obtain a unique set of parameters by such the mode coupling. The cold neutron results reported here and by others [12,13] appear to provide a complete picture of the low-**q** scattering near $(1,1,0)$ and $(1,0,0)$. However, previous thermal-neutron measurements around $(3,0,0)$ and $(1,2,2)$ reported complex cross sections with conflicting interpretations [3,6,7,24]. Thus, further neutron measurements, with high resolution in both $(1,0,0)$ and $(3,0,0)$ zones, are vital for the understanding of the PNR dynamics in PMN.

Acknowledgments

We are very grateful to C. Stock for sharing his PMN data with us before publication. We also thank B. P. Burton, E. J. Cockayne, S. Prosandeev, S. M. Shapiro, S. B. Vakhrushev, and D. Viehland for stimulating discussions. This study was supported by the U.S.-Japan Cooperative Neutron-Scattering Program. Financial support from the U.S. Department of Energy under Contract DE-AC02-98CH10886 is also gratefully acknowledged. Work at SPINS is based upon activities supported by the NSF under DMR-9986442. We also acknowledge the U.S. Dept. of Commerce, NIST Center for Neutron Research, for providing the neutron scattering facilities used in this study.

[1] S. -E. Park and T. R. Shrout, J. Appl. Phys. **82**, 1804 (1997).
[2] Z. -G. Ye, Key Engineering Materials **155-156**, 81 (1998).
[3] A. Naberezhnov, S. Vakhrushev, B. Dorner, D. Strauch, and H. Moudden, Eur. Phys. J. B **11**, 13 (1999).
[4] P. M. Gehring, S. Wakimoto, Z. -G. Ye, and G. Shirane, Phys. Rev. Lett. **87**, 277601 (2001).
[5] S. Wakimoto, C. Stock, R. J. Birgeneau, Z. -G. Ye, W. Chen, W. J. L. Buyers, P. M. Gehring, and G. Shirane, Phys. Rev. B **65**, 172105 (2002).
[6] S. Wakimoto, C. Stock, Z. -G. Ye, P. M. Gehring, and G. Shirane, Phys. Rev. B **66**, 224102 (2002).
[7] S. B. Vakhrushev and S. M. Shapiro, Phys. Rev. B **66**, 214101 (2002).
[8] S. B. Vakhrushev, A. A. Naberezhnov, N. M. Okuneva, and B. N. Savenko, Phys. Solid. State **37**, 1993 (1995).
[9] K. Hirota, Z. -G. Ye, S. Wakimoto, P. M. Gehring, and G. Shirane, Phys. Rev. B **65**, 104105 (2002).
[10] Guangyong Xu, G. Shirane, J. R. D. Copley, and P. M. Gehring, Phys. Rev. B **69**, 064112 (2004).
[11] J. Hlinka, S. Kamba, J. Petzelt, J. Kulda, C. A. Randall, and S. J. Zhang, J. Phys.: Condens. Matter **15**, 4249 (2003).
[12] S. N. Gvasaliya, S. G. Lushnikov, and B. Roessli, cond-mat/0311097.
[13] S. N. Gvasaliya, S. G. Lushnikov, and B. Roessli, Crystallography Reports, **49** 108 (2004).
[14] G. Burns and F. H. Dacol, Solid State Commun. **48**, 853 (1983).
[15] G. Schmidt *et al.*, Krist. und Tech. **15**,1415 (1980).
[16] Z. -G. Ye and H. Schmid, Ferroelectrics **145**, 83 (1993).
[17] H. You and Q. M. Zhang, Phys. Rev. Lett. **79**, 3950 (1997).
[18] N. Takesue, Y. Fujii, and H. You, Phys. Rev. B **64**, 184112 (2001).
[19] B. Chaabane, J. Kreisel, B. Dkhil, P. Bouvier, and M. Mezouar, Phys. Rev. Lett. **90**, 257601, (2003).
[20] C. Stock, H. Luo, D. Vieland, J. F. Li, I. Swainson, R. J. Birgeneau, and G. Shirane, (2004), unpublished. Also private communication by C. Stock.
[21] B. P. Burton and E. Cockayne, Phys. Rev. B **60**, R12542 (1999).
[22] B. P. Burton, J. Phys. Chem. Solids. **61**, 327 (2000).
[23] S. M. Shapiro, J. D. Axe, G. Shirane, and T. Riste, Phys. Rev. B **6**, 4332 (1972).
[24] J. Hlinka, S. Kamba, J. Petzelt, J. Kulda, C. A. Randall, and S. J. Zhang, Phys. Rev. Lett. **91**, 107602 (2003).